metals

MDPI

Article

Rapid Electrodeposition and Corrosion Behavior of Zn Coating from a Designed Deep Eutectic Solvent

Jiayi Chen [1,2], Mengjun Zhu [1,2], Mingtao Gan [1,2], Xiuli Wang [1,2], Changdong Gu [1,2,*] and Jiangping Tu [1,2]

[1] School of Materials Science and Engineering, State Key Laboratory of Silicon Materials, Zhejiang University, Hangzhou 310027, China
[2] Key Laboratory of Advanced Materials and Applications for Batteries of Zhejiang Province, Hangzhou 310027, China
* Correspondence: cdgu@zju.edu.cn; Tel.: +86-13454164563

Abstract: This work aimed to develop a new type of deep eutectic solvent containing high concentrations of zinc ions as an electrolyte to improve the electrodeposition rate for zinc plating. Two typical deep eutectic solvent systems, choline chloride (ChCl)–urea and ChCl–ethylene glycol (EG), were combined to prepare a stable electrolyte at room temperature with a zinc ion concentration up to 2 M. Cyclic voltammetry experiments of the electrolyte at different temperatures were conducted. The effects of key electrodeposition parameters (bath temperature and current density) on the morphology, structure, and corrosion resistance of zinc coatings deposited on mild steel were investigated. It was found that the crystal orientation of the as-deposited zinc particle is related to the electrodeposition temperature and current density. The experimental results show that the zinc coating deposited at 60 °C and the current density of 4 mA·cm^{-2} exhibited the most compact and crack-free morphology, thus had the optimum corrosion resistance property.

Keywords: deep eutectic solvent; electrodeposition; zinc coating; corrosion resistance

Citation: Chen, J.; Zhu, M.; Gan, M.; Wang, X.; Gu, C.; Tu, J. Rapid Electrodeposition and Corrosion Behavior of Zn Coating from a Designed Deep Eutectic Solvent. *Metals* **2023**, *13*, 172. https://doi.org/10.3390/met13010172

Academic Editor: Alberto Moreira Jorge Junior

Received: 4 December 2022
Revised: 11 January 2023
Accepted: 12 January 2023
Published: 14 January 2023

1. Introduction

Ionic liquids (ILs) are salts composed of discrete anions and cations that are molten at, or close to, room temperature [1]. ILs have a wide range of chemical diversity due to the different combinations of anions and cations [2]. ILs have high chemical, thermal stabilities, remarkable solvating power, and extremely high enthalpies of vaporization, which make them effectively nonvolatile [3–7]. Moreover, the electrochemical window of some ILs is very wide (up to 6 V in some cases), making them the superior media for the electrodeposition of active metals and semiconductors [8]. However, there are still some problems that hinder the use of ionic liquids in industry. The synthetic route of ionic liquids is usually too complex and expensive, and often requires toxic or non-renewable reagents [9].

Deep eutectic solvents (DESs) are widely acknowledged as a new generation of room temperature ILs. DESs are systems formed from mixtures of Bronsted or Lewis acids and bases [10]. Due to the formation of hydrogen bonds or coordination bonds, the melting point of DES becomes lower than that of its individual components [11]. DESs and ILs have similar characteristics such as high thermal stabilities, low volatility, low vapor pressures, and tunable polarity [12]. Furthermore, DESs are typically inexpensive, biodegradable, nontoxic, and are easier to prepare [13,14]. Generally, DES is prepared by simply mixing two or more components and stirring at 70 °C or 80 °C without additional purification steps [15]. Due to the above-mentioned superior properties, a large proportion of research work focused on the use of DES as an electrolyte for metal electrodeposition [16–18].

A DES is generally composed of a mixture consisting of a hydrogen bond acceptor (HBA) with a hydrogen bond donor (HBD) [19]. ChCl is widely selected as the HBA, while urea and EG are commonly used as HBDs [20]. The ChCl–urea and ChCl–EG are two typical DES systems applied in the electrodeposition field [21]. However, the low

electrodeposition rate of ChCl-based DES hinders its industrial application. When using ChCl-based DES as the electrolyte, it often takes several hours to electrodeposit a certain thickness of the metal coating [22–24]. The limited solubility of metal ions and the excessive liquid viscosity of ChCl–urea-based electrolytes, which will greatly lower the rate of the mass transport, explain the low electrodeposition rate of ChCl–EG-based electrolytes and ChCl–urea-based electrolytes, respectively [25–27].

Therefore, the interest of the authors is in the challenge of how to improve the electrodeposition rate of ChCl-based DES. Today, zinc coatings are the most widespread method of the protection of mild steel [28]. Thus, in the present work, we focused on how to improve the electrodeposition rate of zinc coatings from the ChCl-based DES. A simple settlement is to mix ChCl–EG and urea to obtain a new DES, which will have both high zinc ion solubility and low viscosity. Through a series of debugging on the mixing ratio of ChCl, EG, urea, and $ZnCl_2$, it was finally determined that the maximum solubility of zinc ions in the solution at room temperature was 2 M. Upon determining the electrolyte, we further explored the influence of key electroplating parameters (bath temperature and current density) on the properties of the deposited zinc layer.

2. Materials and Methods

2.1. Electrolyte Preparation and Zinc Coating Electrodeposition

ChCl ($C_5H_{14}NO{\cdot}Cl$, Shanghai MackLin Biochemical Technology Co., Ltd., Shanghai, China, ≥98%), urea (Shanghai MackLin Biochemical Technology Co., Ltd., ≥99%), and $ZnCl_2$ (Shanghai MackLin Biochemical Technology Co., Ltd., ≥98%) were dried in an oven before use. The schematic diagram of the electrolyte preparation process is shown in Figure S1. The DES (a) was synthesized by mixing ChCl and EG ($C_2H_6O_2$, Sinopharm Chemical Reagent Co., Ltd., >99.5%) in the molar ratio of 1:2. The DES (b) was synthesized by the mixing of $ZnCl_2$ and urea in the molar ratio of 3:10. DES (a) and (b) were both continuously stirred at 70 °C until transparent and homogeneous solutions were obtained. Then, these two solvents were mixed in proportion and the liquid mixture was stirred at the same temperature to obtain a homogeneous solution. The final zinc ion concentration in the DES-based electrolyte was approximately 2 M.

For electrodeposition, Q235 mild steel (MS, thickness: 0.2 mm) served as the cathode substrate and the zinc foil (99.9% pure, thickness: 0.5 mm) was the anode. The surface oxide film of MS was polished by sandpaper. Then, the surface was cleaned by ethanol and dried. When exploring the influence of temperature, a constant current density of 4 $mA{\cdot}cm^{-2}$ was applied by using a DC power source for 15 min. The bath temperatures of room temperature (28 °C, similarly hereinafter), 40 °C, 60 °C, and 80 °C were varied. To explore the influence of current density, the bath temperature was fixed at 60 °C and the current densities of 4, 8, 12, and 16 $mA{\cdot}cm^{-2}$ were varied. In order to reduce the influence of the deposited mass on the coating morphology, it was necessary to keep the deposited electric quantity unchanged at 3.6 $C{\cdot}cm^{-2}$. The detailed electroplating parameters are listed in Table 1 and the electrodeposition time was much shorter than that reported previously.

Table 1. The current densities and deposition time used for the electrodeposition of a zinc coating at 60 °C.

Parameters	Sample A	Sample B	Sample C	Sample D
Current density ($mA{\cdot}cm^{-2}$)	4	8	12	16
Deposition time (min)	15	7.5	5	3.75

After electrodeposition, the sample was thoroughly cleaned with distilled water and ethanol, and then dried in air. All experiments were repeated to avoid accidents.

2.2. Characterization

The cyclic voltammetry experiment of the DES-based electrolyte was performed in a three-electrode system consisting of a Pt working electrode, a Pt counter electrode, and a

Ag wire reference electrode. The cyclic voltammetry experiment was conducted at room temperature, 40 °C, 60 °C, and 80 °C, respectively, and a scan rate of 5 $mV \cdot s^{-1}$. At a relatively low scanning rate (5 $mV \cdot s^{-1}$), the effect of the diffusion mass transfer and the shift of redox peak are small, so the recorded voltammograms will more accurately reflect the characteristics of the reaction itself.

Surface morphology of the zinc coating was characterized using field-emission scanning electron microscopy (Hitachi SU8000). The cross-sectional morphology and distribution of elements were carried out by using energy dispersive spectrometry (EDS, Hitachi s-3400n). An X-ray diffraction (XRD; XPert Pro MPD) experiment was performed in the 2θ range from 10° to 80° to analyze the crystalline structure of zinc coating.

To evaluate the corrosion resistance of different samples, the linear sweep voltammetry (LSV) test and electrochemical impedance spectroscopy (EIS) test were carried out with an electrochemical workstation (CHI660E) in 3.5 wt.% NaCl solution at room temperature. These electrochemical tests were conducted using a three-electrode cell with a Pt plate (6 cm^2) as the counter electrode and a Ag/AgCl electrode as the reference electrode. A sample with a 1 cm × 1 cm exposure area served as the working electrode. Before the LSV test, the sample was immersed in a 3.5 wt.% NaCl solution for about 10 min until a stable open circuit potential (OCP) was obtained. The potentiodynamic curves were recorded from −0.2 V below OCP to +0.2 V above OCP with a scan rate of 1 $mV \cdot s^{-1}$. The EIS test was implemented at the stable OCP. The frequency range was 10^5–10^{-2} Hz, and the AC amplitude was 10 mV.

3. Results and Discussion

3.1. Cyclic Voltammetry Behavior

The electrochemical behavior of the DES electrolyte at different temperatures was studied by cyclic voltammetry (Figure 1). According to the characteristics of the four curves in Figure 1a, we regarded room temperature and 40 °C as low temperatures, while 60 °C and 80 °C as high temperatures. The two cyclic voltammetry curves obtained at low temperature both had only one oxidation peak, located at −0.11 V (28 °C) and 0.05 V (40 °C), respectively. However, the other two cyclic voltammetry curves of the electrolyte measured at high temperature had two oxidation peaks. The first peaks were located at −0.1 V (60 °C) and −0.08 V (80 °C), respectively, and the second peaks were both located around 0.33 V. The difference in the number of oxidation peaks indicates that the electrolyte will show different characteristics at different temperatures. According to A.P. Abbott's experimental results [29], two stripping peaks could be observed in the anodic portions of the voltammogram of the EG-based liquid. In contrast, only a single stripping peak could be observed in the voltammogram of the urea-based liquid. Therefore, at low temperature, the electrolyte shows the characteristics of a urea-based liquid. At high temperature, the electrolyte showed the characteristics of an EG-based liquid.

From Figure 1a, the cathodic portion of the voltammogram showed no well-defined reduction peak. At high temperatures (60 °C and 80 °C), there was no nucleation loop observed in the cathodic portion of the scans. This is consistent with the characteristics of an EG-based liquid, which has slow nucleation and fast bulk growth [29]. At low temperatures (28 °C and 40 °C), a cathodic current cross-over in the voltammogram was observed. This is consistent with the features of a urea-based liquid that has fast nucleation and slow bulk growth [29].

Furthermore, it is clear from Figure 1a that the magnitude of current was more significant at 80 °C than that at room temperature. This was attributed to the fast mass transport in the electrolyte enabled by the low viscosity at high temperature.

3.2. Crystal Structure of Deposited Zinc Coating

In order to determine the crystal structure of metal zinc deposited under different electroplating parameters, XRD tests were carried out for each zinc coating. Only representative results are presented here for illustration.

XRD patterns of the as-deposited zinc coating at low temperature (28 °C) and high temperature (60 °C) are displayed in Figure 2a,b, respectively. The diffraction peaks at 44.7° and 65.0° correspond to the substrate Fe.

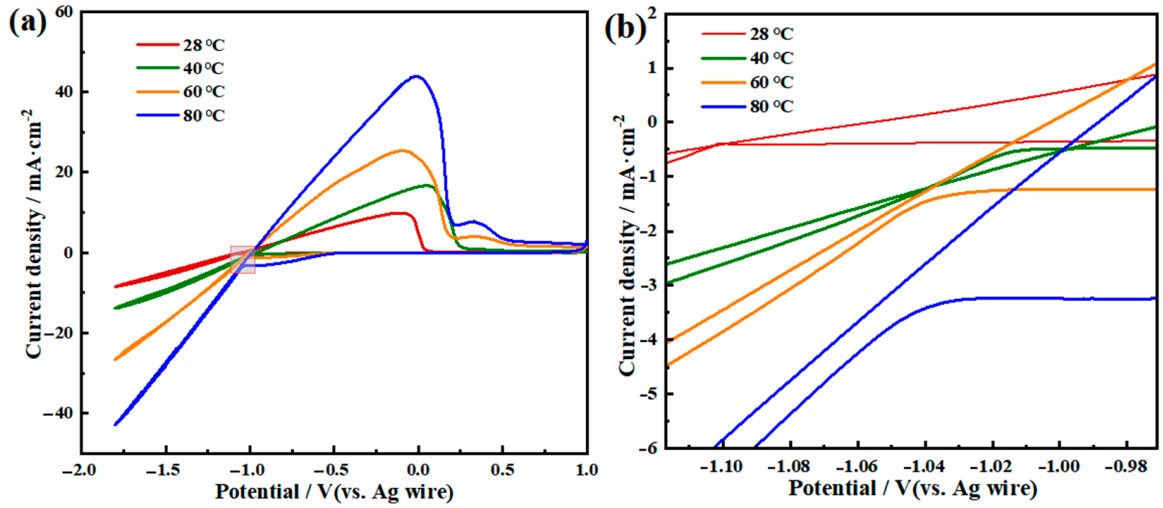

Figure 1. (**a**) Cyclic voltammogram for the DES electrolyte at different temperatures (28 °C, 40 °C, 60 °C, and 80 °C) on a Pt electrode, and (**b**) enlarged view of the cathodic portion.

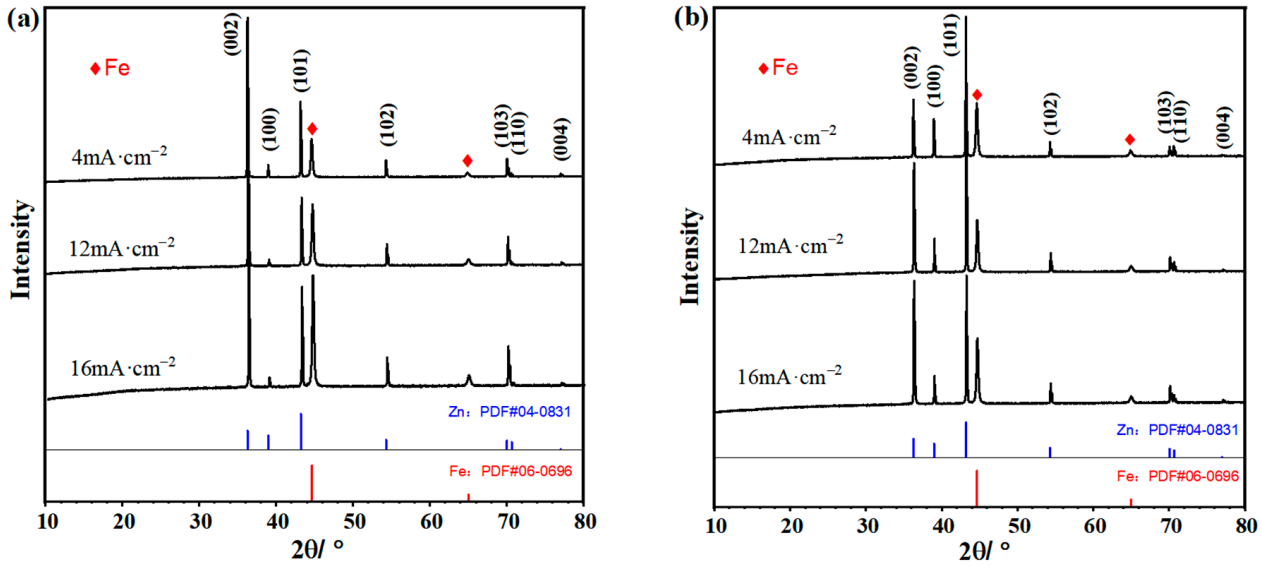

Figure 2. XRD patterns of the zinc deposits from (**a**) 28 °C and (**b**) 60 °C at different current densities.

3.2.1. Influence of Temperature

The XRD pattern of the zinc coating changed greatly with the change in temperature. In Figure 2a, the strongest peak of the as-deposited zinc was the diffraction peak of the (002) crystal plane, while in Figure 2b, the strongest peak corresponded to the (101) crystal plane. Metallic zinc is a typical hexagonal close-packed structure. Among (002), (100) and (101) crystal planes, the preferred exposed crystal planes determine the final morphology of newly deposited zinc metal [30]. Specifically, when the preferred crystal plane is (002), the as-deposited zinc sheet tends to grow at a small angle (about 0°~30°) with the substrate, which makes the zinc metal have a deposition morphology parallel to the substrate. When the (100) and (101) crystal planes are dominant, the as-deposited zinc sheet tends to grow at a large angle (about 70°~90°) with the substrate [31]. Therefore, the zinc sheet deposited at low temperature tends to grow parallel to the substrate, since the dominant crystal plane

is (002). At high temperature, in contrast, the deposited zinc sheet tends to grow at a large angle with the substrate because of the dominant crystal plane of (101).

3.2.2. Influence of Current Density

Both Figure 2a,b show that the change in the current density will not cause a change in the strongest peak in the XRD pattern, that is, the dominant crystal plane of zinc will not change. It is worth noting that in Figure 2a, with the increase in current density, the diffraction peak intensity of the crystal plane (101) increases. In Figure 2b, the diffraction peak intensity of crystal plane (002) also increases with the increase in the current density. In other words, the increase in the current density will make the exposure probability of different crystal planes in the electrodeposition process gradually close.

3.3. Surface Morphology and Coating Thickness

3.3.1. Influence of Temperature on Morphology

The variation in the surface morphology of the zinc electrodeposited at a current density of 4 mA·cm^{-2} at different temperatures is shown in Figure 3, which shows that the zinc deposited at different temperatures is regular massive particles, and the zinc film is uniform but not smooth.

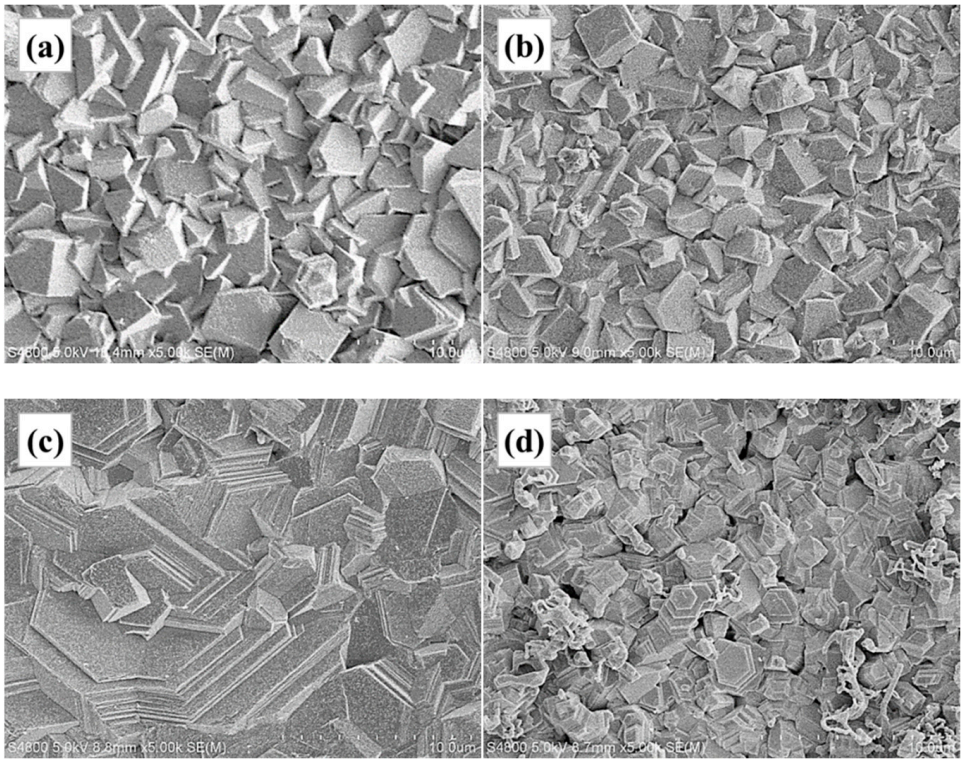

Figure 3. SEM images of the zinc films electrodeposited at 4 mA·cm^{-2} and the temperature of (**a**) 28 °C, (**b**) 40 °C, (**c**) 60 °C, and (**d**) 80 °C, respectively.

According to Figure 3a,b, the surface of the zinc particles electrodeposited at low temperature (28 °C and 40 °C) was flat, while in Figure 3c,d, when electrodeposited at high temperature (60 °C and 80 °C), the surface of the zinc particles had a step-like structure. This is consistent with the XRD characterization results. As above-mentioned, zinc flakes tend to grow parallel to the substrate at low temperatures, thus, we observed zinc particles with flat surfaces. When electroplating at high temperature, the zinc sheet grew at a large angle with the substrate, so a layered step-like structure could be seen under the scanning electron microscope.

We know that the zinc films growing parallel to the substrate should be flatter and denser than those growing at a large angle with the substrate [32]. However, the SEM images show that the zinc coating electrodeposited at 60 °C was the flattest and most compact. This may be related to the property of the DES-based electrolyte. According to the analysis of the cyclic voltammetry curve above, the electrolyte at low temperature showed the characteristics of the ChCl–urea system. In ChCl–urea, the deposition of zinc is characterized by fast nucleation and slow growth. In this case, the size of the zinc particles obtained by electrodeposition is small, about 2 to 3 µm. At a relatively high temperature (60 °C), the electrolyte showed the characteristics of the ChCl–EG system. In ChCl–EG, the deposition of zinc was characterized by slow nucleation and fast growth. Therefore, no isolated zinc particles could be seen in Figure 3c. At 80 °C, since the temperature is too high, the electrolyte or a small part of water in the electrolyte will decompose and generate bubbles during the electroplating process, resulting in a non-compact zinc film (Figure 3d).

3.3.2. Influence of Current Density on Morphology

The variation in the surface morphology of zinc electrodeposited at 60 °C at different current densities is shown in Figure 4.

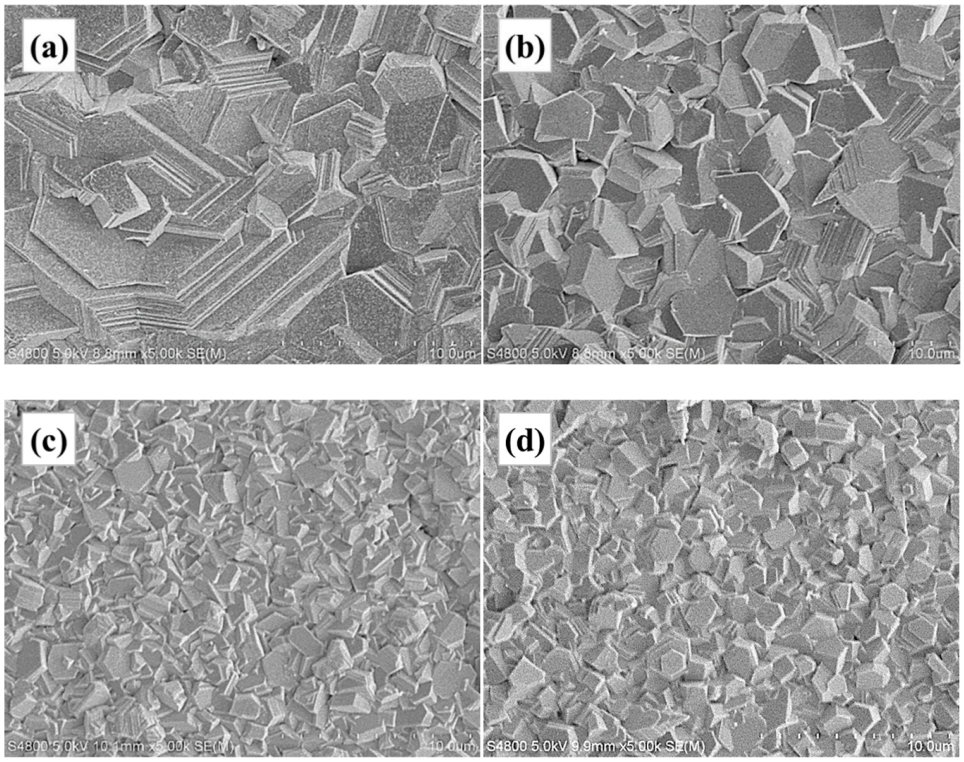

Figure 4. The SEM images of the zinc films electrodeposited at 60 °C and the current density of (**a**) 4 mA·cm^{-2}, (**b**) 8 mA·cm^{-2}, (**c**) 12 mA·cm^{-2}, and (**d**) 16 mA·cm^{-2}, respectively.

It can be seen in Figure 4 that the variation in the current density had two aspects of influence on the zinc coating. On hand, with the increase in the current density, the size of the zinc particles decreased. On the other hand, the increase in the current density reduced the surface flatness of the zinc film. Figure 2b shows that with the increase in the current density, the deposited zinc will change from a state dominated by (101) crystal planes to a state with similar proportions of (101) and (002) planes. The crisscross of crystal planes with different orientations leads to the irregularity of the zinc film.

3.3.3. Coating Thickness

Figure 5 shows several representative cross-section SEM images of the samples after electrodeposition with different electroplating parameters. The blue EDS curves in the

figures represent the distribution of metal zinc, which can illustrate the thickness of the zinc coating. Figure 5a shows that at room temperature, the thickness of the zinc coating could reach 14.7 µm with only 15 min of electrodeposition with a current density of 4 mA·cm^{-2}. In previous reports [33–36], as shown in Table S1, the electrodeposition rate of ChCl-based DES was very slow, and most of them needed to be carried out at high temperature. However, our new DES electrolyte had a much faster electrodeposition rate at room temperature.

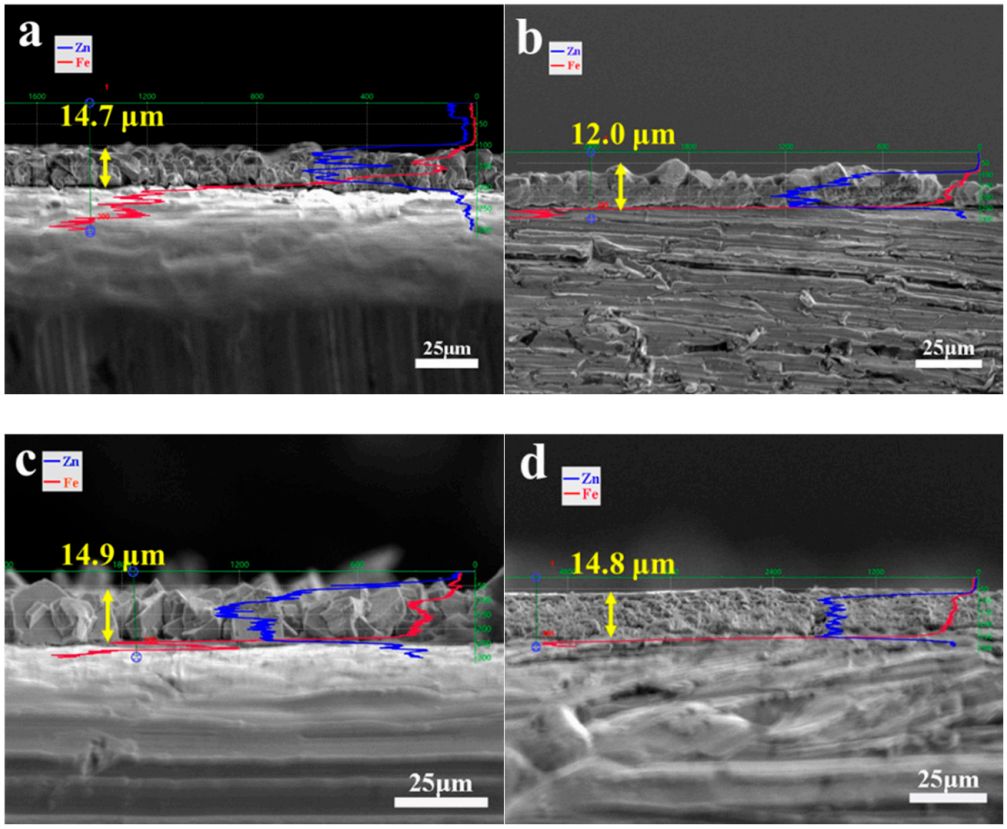

Figure 5. The SEM images containing EDS element distribution curves of cross-sectional samples after electrodeposition with different electroplating parameters of (**a**) 4 mA·cm^{-2}, 28 °C, (**b**) 4 mA·cm^{-2}, 60 °C, (**c**) 16 mA·cm^{-2}, 28 °C, (**d**) 16 mA·cm^{-2}, 60 °C.

Except for Figure 5b, the thickness of the zinc coatings in the other figures was similar. All experiments fixed the deposition electric quantity at 3.6 C. Hence, we can consider that the difference in the deposition rate for different temperatures and different current densities was quite gentle. The zinc coating in Figure 5b was the thinnest. However, the cross-section morphology shows that it was the densest zinc film. In conclusion, it is reasonable to speculate that the deposited mass under different electroplating parameters is similar. In the case of there being little difference in the deposited mass, the following discussion on the corrosion resistance of the zinc coating can be carried out.

3.4. Electrochemical Tests

3.4.1. Influence of Temperature

The corrosion resistance of zinc coatings deposited at different temperatures was investigated by a Tafel polarization curve (Figure 6). The fitting parameters listed in Table 2 such as corrosion potential (E_{corr}), corrosion current (i_{corr}), anodic Tafel slope (β_a), cathodic Tafel slope (β_c), and the polarization resistance (R_p) were used to evaluate the corrosion resistance of the zinc coatings.

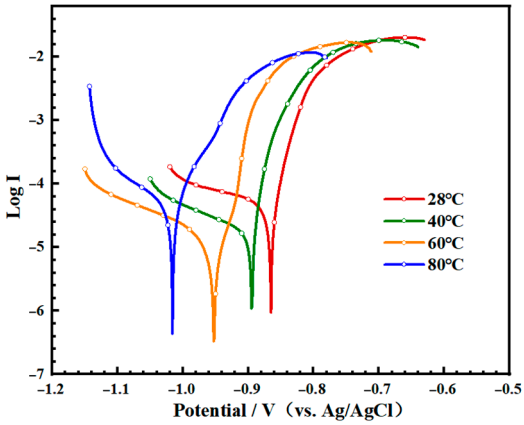

Figure 6. Polarization curves of the zinc films deposited at the current density of 4 mA·cm^{-2} and different temperatures.

Table 2. Data from the polarization curves of the zinc films deposited at the current density of 4 mA·cm^{-2} and at different temperatures.

Samples	E_{corr} (mV)	i_{corr} (μA·cm^{-2})	β_a (mV/dec)	$-\beta_c$ (mV/dec)	R_p (Ω·cm^2)
28 °C	−864	42.9	26.89	369.13	253.69
40 °C	−897	17.4	27.84	237.68	621.90
60 °C	−941	10.9	30.61	193.86	1053.11
80 °C	−1014	41.5	48.37	140.68	376.61

The results show that by increasing the electrodeposition temperature, the curves shifted toward more negative E_{corr} values. This indicates that the reaction activity of the metal zinc obtained by electroplating at high temperature was stronger compared with those deposited at low temperature.

Furthermore, the i_{corr} and R_p values both decreased first and then increased with the increase in the electrodeposition temperature. It was notable that the zinc coating deposited at 60 °C had the minimum corrosion current density (5.01 μA·cm^{-2}). The R_p value of the zinc coating deposited at 60 °C was 1053.11 Ω·cm^2, which was much higher than that deposited at room temperature. As mentioned in Section 3.3.1, when the electrodeposition temperature was 60 °C, the zinc coating obtained had the minimum porosity. The smaller the porosity, the stronger the shielding effect of the coating on the substrate, and the greater the polarization resistance. Therefore, in combination with the variation law of the i_{corr} and R_p values, we can conclude that a dense and compact zinc film can significantly reduce the rate of the anodic reaction and provide better barrier protection for the substrate.

EIS was also used to evaluate the corrosion resistance of the zinc coatings. Figure 7a shows the Nyquist plots of the samples and the four different zinc coatings exhibited a similar semi-circle pattern, which indicates that the coatings had the same electrochemical corrosion mechanism [37]. Radius of the capacitive loop is related to the charge transfer resistance value of the coating. The larger the capacitance loop radius, the greater the charge transfer resistance, and the better the corrosion resistance of the coating [38]. It is clear that the zinc coating deposited at 60 °C had the largest semicircle radius, indicating that it had the optimum corrosion protection performance.

Bode plots (|Z| and phase angle vs. frequency) of the different zinc coatings are shown in Figure 7b,c. In the Bode impedance plot, the higher the impedance modulus in the low-frequency region, the better the corrosion resistance of the coating [39]. From Figure 7b, it can be confirmed that the zinc coating deposited at 60 °C exhibited the highest impedance value, which shows the high corrosion resistance of this coating. The Bode phase plot (Figure 7c) showed one broad peak, which represents the capacitive loop in Nyquist plots [40]. The increased phase angle indicates the increased capacitive nature of the deposited coating and the increased corrosion resistance. It can be seen from the

Bode phase plot that the phase angle of the zinc coating increased with the increase in the electrodeposition temperature.

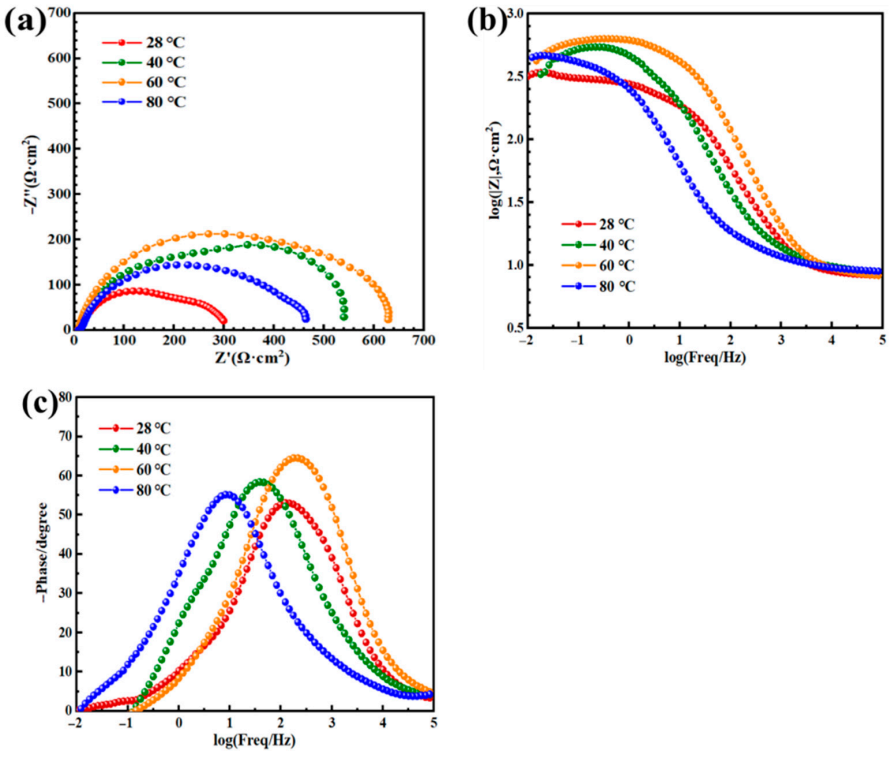

Figure 7. (**a**) Nyquist plots, (**b**) Bode impedance plots, and (**c**) Bode phase plots of the zinc films deposited at the current density of 4 mA·cm^{-2} and at different temperatures.

3.4.2. Influence of Current Density

The corrosion resistance of zinc coatings deposited at different current densities was investigated by Tafel polarization curves (Figure 8). The Tafel fitting parameters are given in Table 3.

From Figure 8, it was observed that the Tafel curves of different zinc coatings were very close to each other. In this case, it can be inferred that the current density had little effect on the corrosion resistance of the zinc coatings.

According to Table 3, the E_{corr} values of the zinc films electrodeposited at different current densities were almost the same, indicating that the current density does not affect the reactivity of the deposited metal. Nevertheless, the current density had an influence on the i_{corr} and R_p values of the zinc coatings. When the current density was 4 mA·cm^{-2}, the i_{corr} value of the zinc coating was about 10.9 μA·cm^{-2} and the R_p value was about 1053.11 Ω·cm^2. When the current density increased to 16 mA·cm^{-2}, the i_{corr} value of the coating increased to 35.9 μA·cm^{-2} and the R_p value decreased to 269.96 Ω·cm^2. As mentioned in Section 3.3.2, the zinc particles obtained by electrodeposition under high current density were more disordered and the coating was not dense enough. As a result, the zinc coating electrodeposited at the current density of 16 mA·cm^{-2} had the worst corrosion protection performance.

EIS was used to further evaluate the corrosion resistance of the zinc coatings. Figure 9a displays the Nyquist plots of the coatings. Among the four Nyquist plots, the plot for the zinc coating deposited at 4 mA·cm^{-2} had the maximum semicircle radius. Radius of the capacitive loop decreased with the increase in the current density. The Bode impedance plots and Bode phase plots are shown in Figure 9b,c. From the figures, it can be seen that with the increase in the current density, both the impedance value in the low frequency region and phase angle of zinc coating decreased. Therefore, at the same electrodeposition temperature, the lower the current density, the better the corrosion resistance of the coating.

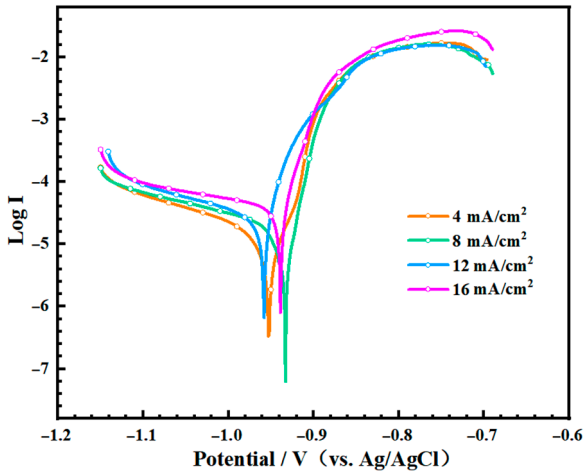

Figure 8. Polarization curves of the zinc films deposited at 60 °C and the different current densities.

Table 3. Data from the polarization curves of the zinc films deposited at 60 °C and the different current densities.

Samples	E_{corr} (mV)	i_{corr} (μA·cm^{-2})	β_a (mV/dec)	$-\beta_c$ (mV/dec)	R_p (Ω·cm^2)
4 mA·cm^{-2}	−941	10.9	30.61	193.86	1053.11
8 mA·cm^{-2}	−924	15.3	16.43	259.39	438.51
12 mA·cm^{-2}	−955	24.9	25.49	260.00	404.82
16 mA·cm^{-2}	−935	35.9	23.67	391.23	269.96

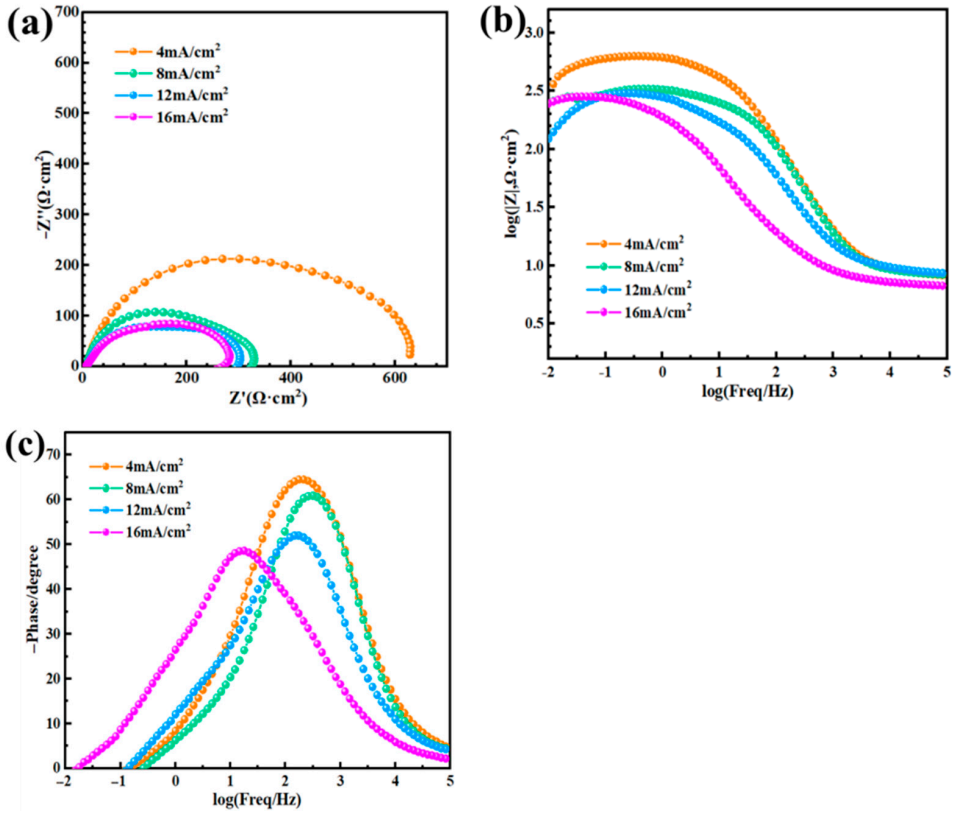

Figure 9. (**a**) Nyquist plots, (**b**) Bode impedance plots, and (**c**) Bode phase plots of the zinc films deposited at 60 °C and at different current densities.

4. Conclusions

In this work, we developed a method to improve the electrodeposition rate of ChCl-based DES and investigated the effects of the electrodeposition temperature and current density on the properties of the zinc coating. Through the analysis of the experimental results, the following conclusions can be derived.

First, the mixture of DES containing 2 M $ZnCl_2$ had a high electrodeposition rate. When the current density was 12 $mA \cdot cm^{-2}$, it only took 5 min to deposit nearly 15 μm of the zinc coating. Regarding the relationship between the electrodeposition temperature and the density of the zinc coating, it was found that in a certain temperature range of 28–60 °C, the higher the temperature, the denser the zinc coating. When the temperature was too high (e.g., 80 °C), the zinc coating density instead decreased. Regarding the current density, there was a negative correlation between the coating density and the current density. Furthermore, the denser the zinc coating, the better the corrosion resistance. The zinc film deposited at 60 °C and 4 $mA \cdot cm^{-2}$ had the optimum corrosion barrier performance. Last but not least, with the increase in the electrodeposition temperature, the E_{corr} value of the zinc coating will move negatively. However, the deposition current density had little effect on the E_{corr} value of the coatings. This work has greatly improved the rate of zinc electrodeposition on a ChCl-based DES, which provides the possibility of the large-scale industrial application of DES in the field of electrodeposition.

Supplementary Materials: The following supporting information can be downloaded at: https://www.mdpi.com/article/10.3390/met13010172/s1, Figure S1: The schematic diagram of the electrolyte preparation process; Table S1: A comparison of electrodeposition rates of ChCl-based DES in previously published work.

Author Contributions: Conceptualization, C.G.; Investigation, J.C.; Resources, C.G., X.W. and J.T.; Data curation, M.Z. and M.G.; Writing—original draft, J.C.; Writing—review & editing, C.G. and J.C. All authors have read and agreed to the published version of the manuscript.

Funding: Zhejiang University K.P. Chao's High Technology Development Foundation.

Data Availability Statement: The data presented in this study are available on request from the corresponding author.

Acknowledgments: This work was supported by Zhejiang University K.P. Chao's High Technology Development Foundation.

Conflicts of Interest: The authors declare no conflict of interest.

References

1. Clarke, C.J.; Tu, W.C.; Levers, O.; Brohl, A.; Hallett, J.P. Green and Sustainable Solvents in Chemical Processes. *Chem. Rev.* **2018**, *118*, 747–800. [CrossRef] [PubMed]
2. Welton, T. Room-temperature ionic liquids. Solvents for synthesis and catalysis. *Chem. Rev.* **1999**, *99*, 2071–2083. [CrossRef] [PubMed]
3. Wilkes, J.S. A short history of ionic liquids—From molten salts to neoteric solvents. *Green Chem.* **2002**, *4*, 73–80. [CrossRef]
4. Armstrong, J.P.; Hurst, C.; Jones, R.G.; Licence, P.; Lovelock, K.R.J.; Satterley, C.J.; Villar-Garcia, I.J. Vapourisation of ionic liquids. *Phys. Chem. Chem. Phys.* **2007**, *9*, 982–990. [CrossRef] [PubMed]
5. Anantharaj, S.; Noda, S.; Driess, M.; Menezes, P.W. The Pitfalls of Using Potentiodynamic Polarization Curves for Tafel Analysis in Electrocatalytic Water Splitting. *Energy Lett.* **2021**, *6*, 1607–1611. [CrossRef]
6. Liu, Y.X.; Liu, Z.; Xu, A.Y.; Liu, X.T. Understanding pitting corrosion behavior of AZ91 alloy and its MAO coating in 3.5% NaCl solution by cyclic potentiodynamic polarization. *J. Magnes. Alloy.* **2022**, *10*, 1368–1380. [CrossRef]
7. Abdelhamid, H.N.; Georgouvelas, D.; Edlund, U.; Mathew, A.P. CelloZIFPaper: Cellulose-ZIF hybrid paper for heavy metal removal and electrochemical sensing. *Chem. Eng. J.* **2022**, *446*, 136614. [CrossRef]
8. Armand, M.; Endres, F.; MacFarlane, D.R.; Ohno, H.; Scrosati, B. Ionic-liquid materials for the electrochemical challenges of the future. *Nat. Mater.* **2009**, *8*, 621–629. [CrossRef]
9. Zhang, Y.; Bakshi, B.R.; Demessie, E.S. Life cycle assessment of an ionic liquid versus molecular solvents and their applications. *Environ. Sci. Technol.* **2008**, *42*, 1724–1730. [CrossRef]

10. Zhang, Q.; Vigier, K.D.O.; Royer, S.; Jerome, F. Deep eutectic solvents: Syntheses, properties, and applications. *Chem. Soc. Rev.* **2012**, *41*, 7108–7146. [CrossRef]
11. Svigelj, R.; Dossi, N.; Grazioli, C.; Toniolo, R. Deep Eutectic Solvents (DESs) and Their Application in Biosensor Development. *Sensors* **2021**, *21*, 4263. [CrossRef]
12. Halder, A.K.; Natalia, M.; Cordeiro, D.S. Probing the Environmental Toxicity of Deep Eutectic Solvents and Their Components: An In Silico Modeling Approach. *ACS Sustain. Chem. Eng.* **2019**, *7*, 10649–10660. [CrossRef]
13. Khandelwal, S.; Tailor, Y.K.; Kumar, M. Deep eutectic solvents (DESs) as eco-friendly and sustainable solvent/catalyst systems in organic transformations. *J. Mol. Liq.* **2016**, *215*, 345–386. [CrossRef]
14. Xu, P.; Zheng, G.W.; Zong, M.H.; Li, N.; Lou, W.Y. Recent progress on deep eutectic solvents in biocatalysis. *Bioresour. Bioprocess.* **2017**, *4*, 34. [CrossRef]
15. Hansen, B.B.; Spittle, S.; Chen, B.; Poe, D.; Zhang, Y.; Klein, J.M.; Horton, A.; Adhikari, L.; Zelovich, T.; Doherty, B.W.; et al. Deep Eutectic Solvents: A Review of Fundamentals and Applications. *Chem. Rev.* **2021**, *121*, 1232–1285. [CrossRef]
16. Abbott, A.P.; Ballantyne, A.; Harris, R.C.; Juma, J.A.; Ryder, K.S. Bright metal coatings from sustainable electrolytes: The effect of molecular additives on electrodeposition of nickel from a deep eutectic solvent. *Phys. Chem. Chem. Phys.* **2017**, *19*, 3219–3231. [CrossRef]
17. Bernasconi, R.; Lucotti, A.; Nobili, L.; Magagnin, L. Ruthenium Electrodeposition from Deep Eutectic Solvents. *J. Electrochem. Soc.* **2018**, *165*, D620–D627. [CrossRef]
18. Protsenko, V.; Bobrova, L.; Danilov, F. Trivalent chromium electrodeposition using a deep eutectic solvent. *Anti-Corros. Methods Mater.* **2018**, *65*, 499–505. [CrossRef]
19. Li, X.; Lee, Y.R.; Row, K.H. Synthesis of Mesoporous Siliceous Materials in Choline Chloride Deep Eutectic Solvents and the Application of These Materials to High-Performance Size Exclusion Chromatography. *Chromatographia* **2016**, *79*, 375–382. [CrossRef]
20. Abbott, A.P.; Capper, G.; Davies, D.L.; Rasheed, R.K.; Tambyrajah, V. Novel solvent properties of choline chloride/urea mixtures. *Chem. Commun.* **2003**, *1*, 70–71. [CrossRef]
21. Smith, E.L.; Abbott, A.P.; Ryder, K.S. Deep Eutectic Solvents (DESs) and Their Applications. *Chem. Rev.* **2014**, *114*, 11060–11082. [CrossRef] [PubMed]
22. You, Y.H.; Gu, C.D.; Wang, X.L.; Tu, J.P. Electrochemical Synthesis and Characterization of Ni-P Alloy Coatings from Eutectic-Based Ionic Liquid. *J. Electrochem. Soc.* **2012**, *159*, D642–D648. [CrossRef]
23. Fashu, S.; Gu, C.D.; Zhang, J.L.; Huang, M.L.; Wang, X.L.; Tu, J.P. Effect of EDTA and NH_4Cl additives on electrodeposition of Zn-Ni films from choline chloride-based ionic liquid. *Trans. Nonferrous Met. Soc.* **2015**, *25*, 2054–2064. [CrossRef]
24. Yanai, T.; Shiraishi, K.; Shimokawa, T.; Watanabe, Y.; Ohgai, T.; Nakano, M.; Suzuki, K.; Fukunaga, H. Electroplated Fe films prepared from a deep eutectic solvent. *J. Appl. Phys.* **2014**, *115*, 17A344. [CrossRef]
25. Whitehead, A.H.P. Matthias Gollas, Bernhard, Zinc Electrodeposition from a Deep Eutectic System Containing Choline Chloride and Ethylene Glycol. *J. Electrochem. Soc.* **2010**, *157*, D328–D334. [CrossRef]
26. Fashu, S.; Khan, R. Electrodeposition of ternary Zn-Ni-Sn alloys from an ionic liquid based on choline chloride and their characterisation. *Trans. IMF* **2016**, *94*, 237–245. [CrossRef]
27. Hu, L.; Luo, J.; Lu, D.; Tang, Q. Urea decomposition: Efficient synthesis of pyrroles using the deep eutectic solvent choline chloride/urea. *Tetrahedron Lett.* **2018**, *59*, 1698–1701. [CrossRef]
28. Hu, C.; Xie, X.; Zheng, H.; Qing, Y.; Ren, K. Facile fabrication of superhydrophobic zinc coatings with corrosion resistance via an electrodeposition process. *New J. Chem.* **2020**, *44*, 8890–8901. [CrossRef]
29. Abbott, A.P.; Barron, J.C.; Ryder, K.S. Electrolytic deposition of Zn coatings from ionic liquids based on choline chloride. *Trans. IMF* **2013**, *87*, 201–207. [CrossRef]
30. Li, Y.; Wu, P.; Zhong, W.; Xie, C.; Xie, Y.; Zhang, Q.; Sun, D.; Tang, Y.; Wang, H. A progressive nucleation mechanism enables stable zinc stripping-plating behavior. *Energy Environ. Sci.* **2021**, *14*, 5563–5571. [CrossRef]
31. Wang, T.; Sun, J.; Hua, Y.; Krishna, B.N.V.; Xi, Q.; Ai, W.; Yu, J.S. Planar and dendrite-free zinc deposition enabled by exposed crystal plane optimization of zinc anode. *Energy Storage Mater.* **2022**, *53*, 273–304. [CrossRef]
32. Zou, J.; Zeng, Z.; Wang, C.; Zhu, X.; Zhang, J.; Lan, H.; Li, L.; Yu, Y.; Wang, H.; Zhu, X.; et al. Ultraconformal Horizontal Zinc Deposition toward Dendrite-Free Anode. *Small Struct.* **2022**, *4*, 2200194. [CrossRef]
33. Alesary, H.F.; Cihangir, S.; Ballantyne, A.D.; Harris, R.C.; Weston, D.P.; Abbott, A.P.; Ryder, K.S. Influence of additives on the electrodeposition of zinc from a deep eutectic solvent. *Electrochim. Acta* **2019**, *304*, 118–130. [CrossRef]
34. Gu, C.D.; You, Y.H.; Yu, Y.L.; Qu, S.X.; Tu, J.P. Microstructure, nanoindentation, and electrochemical properties of the nanocrystalline nickel film electrodeposited from choline chloride-ethylene glycol. *Surf. Coat. Technol.* **2011**, *205*, 4928–4933. [CrossRef]
35. Yang, H.Y.; Guo, X.W.; Chen, X.B.; Wang, S.H.; Wu, G.H.; Ding, W.J.; Birbilis, N. On the electrodeposition of nickel-zinc alloys from a eutectic-based ionic liquid. *Electrochim. Acta* **2012**, *63*, 131–138. [CrossRef]
36. Bakkar, A.; Neubert, V. Electrodeposition onto magnesium in air and water stable ionic liquids: From corrosion to successful plating. *Electrochem. Commun.* **2007**, *9*, 2428–2435. [CrossRef]
37. Wang, S.Y.; Si, N.C.; Xia, Y.P.; Liu, L. Influence of nano-SiC on microstructure and property of MAO coating formed on AZ91D magnesium alloy. *Trans. Nonferrous Met. Soc.* **2015**, *25*, 1926–1934. [CrossRef]

38. Riyas, A.H.; Geethanjali, C.V.; Shibli, S.M.A. Tuning of η-phase layer with Zr/Al content to enhance corrosion resistance of zinc coating. *Mater. Sci. Eng. B* **2022**, *277*, 115609. [CrossRef]
39. Raja, V.S.; Panday, C.K.; Saji, V.S.; Vagge, S.T.; Narasimhan, K. An electrochemical study on deformed galvanneal steel sheets. *Surf. Coat. Tech.* **2006**, *201*, 2296–2302. [CrossRef]
40. McIntyre, J.M.; Pham, H.Q. Electrochemical impedance spectroscopy; A tool for organic coatings optimizations. *Prog. Org. Coat.* **1996**, *27*, 201–207. [CrossRef]